

Article

Analysis of the Vigor of *Pinus hartwegii* Lindl. along an Altitudinal Gradient Using UAV Multispectral Images: Evidence of Forest Decline Possibly Associated with Climatic Change

José Luis Gallardo-Salazar ¹, Roberto A. Lindig-Cisneros ², Leonel Lopez-Toledo ³, Angel R. Endara-Agramont ⁴ , Arnulfo Blanco-García ⁵ and Cuauhtémoc Sáenz-Romero ^{3,*} 

¹ Instituto de Investigaciones Agropecuarias y Forestales, Universidad Michoacana de San Nicolás de Hidalgo (UMSNH), Morelia 58330, Michoacán, Mexico; 2251351x@umich.mx

² Instituto de Investigaciones en Ecosistemas y Sustentabilidad, Universidad Nacional Autónoma de México (UNAM), Morelia 58190, Michoacán, Mexico; rlindig@iies.unam.mx

³ Instituto de Investigaciones sobre los Recursos Naturales, Universidad Michoacana de San Nicolás de Hidalgo (UMSNH), Morelia 58330, Michoacán, Mexico; leonel.lopez@umich.mx

⁴ Instituto de Ciencias Agropecuarias y Rurales (ICAR), Universidad Autónoma del Estado de México, Instituto Literario No. 100, Col. Centro, Toluca 50000, Estado de México, Mexico; arendaraaa@uaemex.mx

⁵ Facultad de Biología, Universidad Michoacana de San Nicolás de Hidalgo (UMSNH), Morelia 58030, Michoacán, Mexico; arnulfo.blanco@umich.mx

* Correspondence: cuauhtemoc.saenz@umich.mx; Tel.: +52-443-271-9388



Citation: Gallardo-Salazar, J.L.; Lindig-Cisneros, R.A.; Lopez-Toledo, L.; Endara-Agramont, A.R.; Blanco-García, A.; Sáenz-Romero, C. Analysis of the Vigor of *Pinus hartwegii* Lindl. along an Altitudinal Gradient Using UAV Multispectral Images: Evidence of Forest Decline Possibly Associated with Climatic Change. *Forests* **2023**, *14*, 1176. <https://doi.org/10.3390/f14061176>

Academic Editors: Nadezhda Tchekabakova and Sergey V. Verkhovets

Received: 6 April 2023

Revised: 3 June 2023

Accepted: 4 June 2023

Published: 6 June 2023



Copyright: © 2023 by the authors. Licensee MDPI, Basel, Switzerland. This article is an open access article distributed under the terms and conditions of the Creative Commons Attribution (CC BY) license (<https://creativecommons.org/licenses/by/4.0/>).

Abstract: Future climate forecasts predict major changes that will have negative impacts on the distribution, abundance, and dynamics of forest ecosystems. In Mexico, there is evidence of symptoms of massive forest decline; however, there is no consensus in terms of attributing these symptoms to climate change. This study aimed to provide evidence of forest decline possibly associated with climatic change in the highland pine (*Pinus hartwegii* Lindl.) populations of the Nevado de Toluca Flora and Fauna Protection Area. Using unmanned aerial vehicles (UAV) equipped with multispectral sensors, the study applied digital photogrammetry techniques, automated tree crown detection algorithms, and calculation of the normalized difference vegetation index (NDVI) and leaf chlorophyll index (LCI) to assess forest health across an altitudinal transect (from 3300 m to the timberline at 4040 m elevation). Climate analysis was conducted with TerraClimate data using mean annual temperature (MAT), April temperature, and Palmer Drought Severity Index (PDSI) from the studied altitudinal transect and its xeric limit. We found that lower altitude populations had significantly higher stress levels, indicating forest decline phenomena, while intermediate altitude populations showed greater vigor of the detected trees. Statistically significant differences in the NDVI and LCI values along the altitudinal gradient provided evidence of forest decline in terms of forest vigor and productivity, with the greatest disturbance found at the lower altitude of the examined forest species. The analysis of the climatic data revealed an increase in April temperature $+1.4^{\circ}\text{C}$ of the xeric limit of the transect (low altitude) when comparing the reference period, 1961–1990 (mean: 12.17°C), with the decade prior to our study (2011–2020; mean: 13.57°C). This would be equivalent to an upward shift in elevation of 280 m of the xeric limit. In addition, the PDSI analysis revealed that droughts are becoming increasingly intense at a rate of 0.06 PDSI units per decade, with greater intensity in the last five years. These findings highlight the negative impacts of climate change on forest ecosystems and the urgent need for alternative forest management and conservation practices to increase resilience and adaptation in the temperate forests of Mexico. This study sets a precedent for further research to improve our understanding of the impacts of climate change on forest ecosystems and the development of sustainable management practices.

Keywords: droughts; NDVI; LCI; xeric limit; unmanned aerial vehicles

1. Introduction

Pinus hartwegii Lindl., commonly known as “highland pine”, represents one of the highest altitudinal limits of arboreal vegetation worldwide [1]. It grows along an altitudinal gradient primarily ranging from 3000 to 4000 m in elevation in various mountainous areas of Mexico and Central America [1,2]. One notable characteristic of this species is its tolerance to the low temperatures typically found in high mountain ecosystems [3,4]. Consequently, its extreme altitudinal distribution makes it highly vulnerable to climate change [5] because it does not have available areas at higher altitudes to which it can migrate, as its higher altitude populations are often close to mountain summits. Similar to forests in other parts of the world, the *P. hartwegii* forests have been largely shaped by climatic conditions [6,7]. The climate has now become warmer and is projected to undergo even more changes and at an unprecedented rate [8]. It is anticipated that the plant species in mountain ecosystems will undergo changes in their distribution, abundance, and population dynamics [9–11], which could compromise the region’s high biodiversity and the environmental services they provide [12].

Climate change scenarios suggest that the combination of increased temperature and decreased precipitation will lead to a more arid climate in Mexico [13]. Climate change-related impacts are global and appear to be growing in intensity and frequency [14]. Evidence of this can be seen in the stress symptoms presented by 23% of the world’s forests, which compromise their resilience to climate change [15]. For example, the forests of the southwestern USA have experienced the unprecedented death of more than 100 million trees [16,17]. Furthermore, Allen et al. [18] state that drought and heat events in the southwestern USA have caused extensive insect outbreaks and mortality in many forest types, affecting 20 million hectares. Between California and Texas, nearly half a billion trees have died since 2010 as a result of this phenomenon [14]. These threats are projected to be more critical at the lower limits of species distribution, such as the xeric boundaries, as these areas are associated with higher temperatures and arid conditions [19–21].

Given the extensive nature of the ongoing forest decline events [11,22] and the high cost associated with assessing them through field surveys, the utilization of remotely sensed information has become necessary [23]. For more than three decades, forest decline associated with climate change has been studied using satellite platforms [24]. However, satellite-based information is limited to regional or global scale studies due to its now low resolution and interference from atmospheric factors (such as cloud cover) that diminish its quality [25]. The incorporation of new technologies such as unmanned aerial vehicles (UAV), commonly known as “drones”, presents new opportunities to capture information with high spatial, spectral, and temporal resolution in forest ecosystems [26], enabling analysis at the individual tree level of detail [27]. This makes it possible to recognize ecological parameters for the early detection of phytosanitary problems, determination of leaf phenology conditions, and symptoms of forest decline and mortality that are attributable to climate change [28–31].

The use of multispectral cameras mounted on UAVs makes it possible to estimate vegetation indices [32], which are used to monitor variations in the photosynthetic activity of forest populations [33]. These variations are key to identifying signs of stress and defoliation in the crown, which are among the initial symptoms of stress in trees [34]. Spectral indices can analyze physiological changes such as chlorosis, a phenomenon that often precedes forest mortality processes. Therefore, they are therefore considered instrumental in identifying early stages of forest decline [35,36]. The normalized difference vegetation index (NDVI) is a widely used metric that evaluates photosynthetic activity by comparing near-infrared and visible light reflectance. It helps assess vegetation health and monitor changes in plant growth and ecosystem dynamics [37]. Additionally, the leaf chlorophyll index (LCI) has been developed utilizing the red-edge band. LCI serves as a proxy for chlorophyll content [38] and is employed to evaluate stress, disease, and decline in conifers [35].

In Mexico, a recent analysis by Sáenz-Romero et al. [11] provides evidence of symptoms of forest decline attributable to climate change in the Trans-Mexican Volcanic Belt (TMVB) and northwestern Mexico. However, the authors note that there is no consensus in the Mexican forest management community in terms of attributing massive forest decline symptoms to climate change. Given the lack of validated methods in Mexico, the impact of climate change must be urgently quantified to improve the understanding of how forests will respond to this phenomenon [7]. In addition, and with special attention to the xeric boundary, factors such as altitudinal gradient, slope, and aspect must be included in these assessments [19–21].

The Nevado de Toluca Flora and Fauna Protection Area (NTFFPA) constitutes one of the main forest resource reserves in central Mexico [39]. This protected natural area is host to populations of *P. hartwegii*, a species of high commercial value that is adapted to the harsh alpine environment of the high-altitude mountains [40]. This species provides a wide range of ecosystem services to society as recreation opportunities, carbon capture, and water infiltration. However, it is currently threatened due to global warming, with models predicting that its populations would need to migrate to higher altitudes to remain within conditions suitable for growth [41,42]. To achieve this, an upward migration of approximately 400 m in altitudinal is estimated to be necessary to align with the projected climate for the decade centered around the year 2060. However, the summits of the highest mountains in Mexico have limits in altitude and area that, in many cases, preclude such migration, even without considering the fact that natural migration mechanisms are too slow [43]. Therefore, the adaptation of this species to these particular environmental conditions makes it highly vulnerable to the impacts of climate change [44].

To our knowledge, there are no studies that have used vegetation indices calculated with UAVs along an altitudinal gradient to detect stress levels in high mountain ecosystems in Mexico [45]. Therefore, this research aims to provide evidence of possible symptoms of forest decline in the populations of *P. hartwegii* present in the NTFFPA. The objective of this study was to detect differences in the vigor of this species by calculating NDVI and LCI along an altitudinal gradient within the NTFFPA.

The hypothesis was that *P. hartwegii* would present different levels of vigor along the altitudinal gradient, where the greatest forest decline would occur at the xeric limit (sensu Mátyás [19], lower altitudinal limit of the species). In this way, we intended to establish a precedent with which to improve the understanding of climate change impacts and help develop forest management alternatives and targeted conservation practices to increase resilience and adaptation in the temperate forests of Mexico.

2. Materials and Methods

2.1. Study Area

The study site was located on the eastern-facing slope relative to the NTFFPA crater, specifically in a transect along the altitudinal gradient where *P. hartwegii* is distributed. The analyzed forests belong to the municipality of Calimaya in Estado de México. The NTFFPA covers approximately 54,000 hectares [46] and is limited by parallels of $19^{\circ}3'36''$ and $19^{\circ}16'55''$ N and meridians of $99^{\circ}40'37''$ and $99^{\circ}53'56''$ W (Figure 1). It is delimited by the 3000 m rise in elevation toward the summit of the Xinantécatl volcano (known as “Nevado de Toluca”) at 4680 m, which ranks fourth among the highest peaks in Mexico [47]. The dominant soils are andosols [48], and the climate of the region is cold and semi-cold sub-humid, with an average annual rainfall of 1050 mm and an average annual temperature of between -2 and $+7$ °C [46].

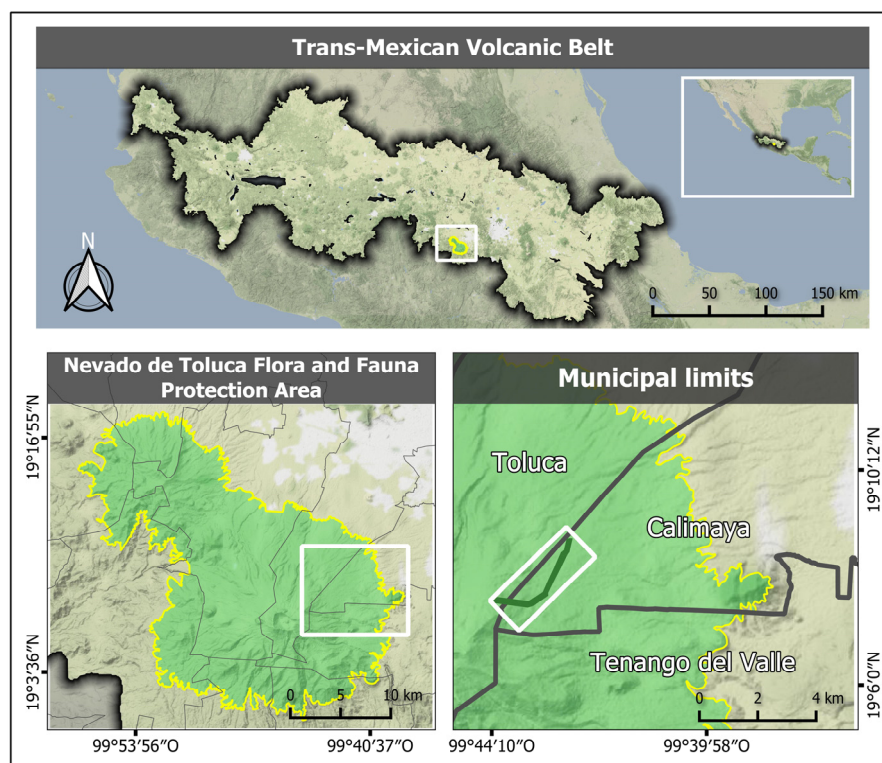


Figure 1. Study area (transect with eastern aspect) in *Pinus hartwegii* forests belonging to the municipality of Calimaya, Estado de México, within the Nevado de Toluca Flora and Fauna Protection Area.

In a regional context, the NTFFPA is part of the TMVB. This region presents high biodiversity and wide climatic and geological variability [49], which serve as a valuable source of ecosystem services (e.g., water supply, carbon sequestration, and biodiversity protection) [50] and confer a strategic value for conservation studies focused on studying the effects of climate change [11,51,52].

2.2. UAV Platform Equipped with a Multispectral Camera

The UAV used was a Phantom 4 Multispectral (P4M) multirotor from Dà-Jiāng Innovations (DJI, Shenzhen, Guangdong, China) (Figure 2). The P4M was equipped with six sensors: one corresponding to visible light spectrum (RGB) and five multispectral sensors (blue, green, red, red-edge, and near-infrared), all with a 2 MP global shutter (see Table S1 of the Supplementary Material) [53]. The P4M had higher accuracy, performance, and consistent data capture compared to other multispectral sensor models [54].

The P4M functions based on the principle of performing geo-referencing directly on board. It was fitted with a global positioning satellite receiver that assigned geographical tags to each captured image using the corresponding coordinates. This indicates that the captured images were georeferenced directly while the flight mission was ongoing [55]. The use of a real-time kinematic (RTK) system was unnecessary because the P4M had a georeferencing system with vertical and horizontal location accuracies of ± 0.1 and ± 0.3 m, respectively [53].



Figure 2. DJI Phantom 4 Multispectral quadcopter used to acquire images, together with the remote control and mobile device (iPad) used to visualize the Ground Station Pro flight application.

2.3. Planning and Execution of Flights along the Altitudinal Gradient

The flight missions were executed on the dates of 7 and 8 April 2022, which coincided with the driest and hottest month of the year in this region of the country [56]. Thus, together with the eastern aspect, the conditions were favorable for evaluating possible symptoms of forest decline. The flight route for capturing images automatically was set using the DJI Ground Station Pro application [57]. To cover the distribution area of *P. hartwegii* in the study site, four connected and consecutive flights were established along the altitudinal gradient, i.e., from 3300 m (lower limit of the dominant distribution of *P. hartwegii*) to 4040 m (upper limit of its dominant distribution). Each of the four flights consisted of a grid approximately 200 m in width with flightpath lengths of 1110, 928, 1680, and 625 m, respectively (Figure 3). The flight was conducted with the followed parameters: 70% frontal and lateral overlap, a flight altitude set at 70 m above ground level (although elevation varied along the flight due to the rough terrain and pronounced slope), and a camera angle of 90°. The flights were conducted under sunny and clear sky conditions (no clouds), as close to noon as possible to avoid shadow interference, and with wind speeds below 5 km/h (see Table S2 of the Supplementary Material).

2.4. Photogrammetric Processing of UAV Images

Photogrammetric and computer vision techniques were employed using RGB and multispectral images, utilizing OpenDroneMap (ODM), a free and open-source software [58]. The results obtained from this software were comparable to those of commercial options. However, ODM offered multiple customization options, shorter processing time, and available documentation, which made it a favorable option [59].

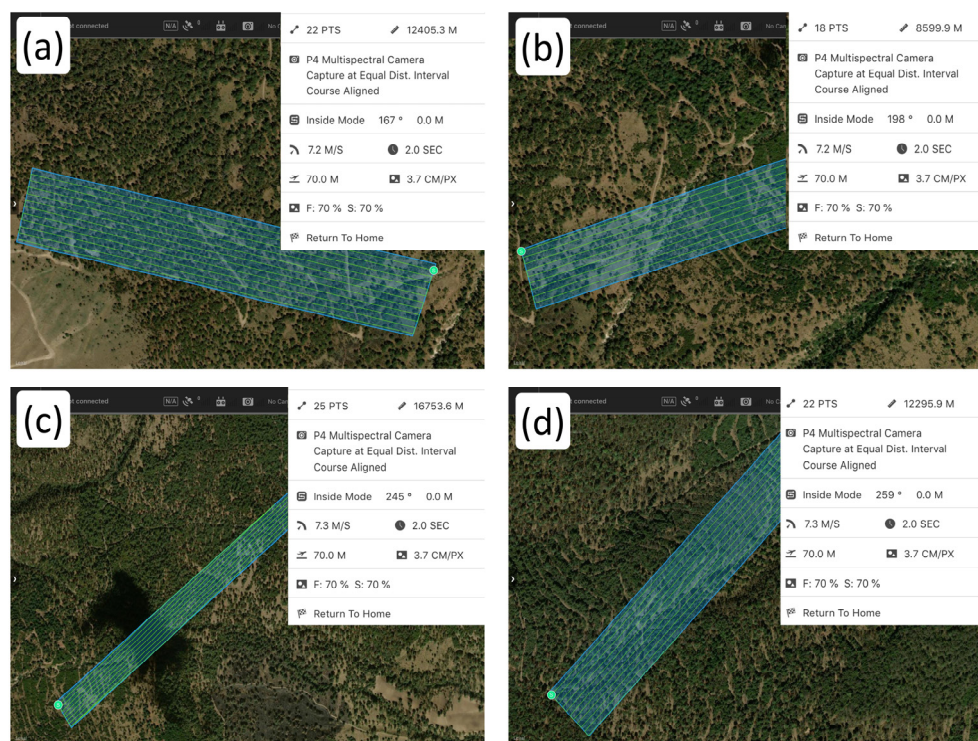


Figure 3. Flight missions programmed with DJI Ground Station Pro along the altitudinal gradient on which *Pinus hartwegii* is distributed: (a) flight covering 4040 to 3700 m; (b) flight covering 3700 to 3560 m; (c) flight covering 3560 to 3400 m; (d) flight covering 3400 to 3300 m.

This software utilizes Structure from Motion (SfM) and Multi-View Stereo (MVS) algorithms to build 3D models from sequences of 2D images that exhibit a substantial level of overlap [60]. Initially, a sparse point cloud is produced using the SfM algorithm, and a dense point cloud is subsequently produced using the MVS algorithm. The dense point cloud with spectral information derived from the input images represents the main output of the UAV photogrammetry workflow [61]. The dense point cloud undergoes classification, filtering, and interpolation procedures to create a digital surface model (DSM) and a digital terrain model (DTM) [62]. These models are subsequently employed to orthorectify individual images and assemble an orthomosaic [63]. This process results in multispectral orthomosaics, DSM, and DTM for the designated study area.

2.5. Calculation of Vegetation Indices

The multispectral orthomosaic generated using the photographs captured with the P4M was utilized to calculate NDVI and LCI using the QGIS 3.28 raster calculator [64]. These vegetation indices are sensitive to changes in the spectral response of trees showing symptoms of forest decline [65]. NDVI is one of the most widely used and implemented indices, and it is calculated from multispectral information as a normalized ratio between the red and near-infrared bands [37]. Mathematically, NDVI is expressed as:

$$\text{NDVI} = \frac{\text{NIR} - \text{RED}}{\text{NIR} + \text{RED}} \quad (1)$$

The normalized difference vegetation index (NDVI) was represented with Equation (1), where RED represents the spectral response captured in the red band and NIR corresponds to the response in the near-infrared range (see Table S1 of the Supplementary Material). NDVI values range from -1 to 1 . Typically, these values are negative for water bodies, close to zero for rock, sand, or concrete surfaces, and positive for vegetation cover (crops, shrubs, grasses, and forests) [37,66]. In other words, NDVI values close to 1 represent more vigorous vegetation and higher photosynthetic activity.

The LCI is a sensitive index for monitoring chlorophyll content in plants [38]. It has been used to assess vegetation growth and productivity [67,68]. It has also been shown to be an indicator for assessing stress, disease, and decline in conifers [35]. Mathematically, LCI is expressed as:

$$LCI = \frac{NIR - RedEdge}{NIR + RED} \quad (2)$$

where LCI is the leaf chlorophyll index, RED is the spectral response recorded with the P4M in the red (visible) band, and NIR and RedEdge are the responses in the near-infrared and red-edge, respectively (see Table S1 of the Supplementary Material). As with NDVI, LCI values range from -1 to 1 , where higher values (1 or closer) indicate higher chlorophyll content, which is related to nitrogen sufficiency in leaves.

2.6. Detection and Extraction of Information at Individual Tree Level

Numerous methods exist for the detection of individual trees in different forest scenarios [69–72]. In the present study, the Tree Density Calculator [73], a plugin to QGIS developed in C++ and PyQGIS, was utilized due to its high efficiency and operational flexibility. This tool is designed to detect tree crowns as a function of image brightness using the local maximum of a sliding window method. This method has been successfully tested in several forestry studies [74,75].

The premise on which the Tree Density Calculator operates is that the tree canopy appears as the brightest part of the tree in remotely sensed images. The tool uses a sliding window that moves over the image, and each window position is verified to determine whether the central pixel is the brightest in the window. If this is the case, the pixel is marked as a local maximum (i.e., tree crown) [73]. In its most basic form, the Tree Density Calculator has only one input parameter, the size of the sliding window, which depends on the resolution of the images and the size of the tree crowns. In the present study, a window size of 15×15 pixels was used. According to Crabbé et al. [73], this method is recommended in coniferous forests due to the shape of their crowns and the characteristics of high-resolution images, such as those provided by the UAV.

After detecting the *P. hartwegii* trees, the respective information was extracted from the calculated vegetation indices (i.e., NDVI and LCI). For each detected tree, a simple zone of influence (buffer) of 4 m in diameter was generated, corresponding to the minimum crown size for dominant trees of this coniferous species [76]. Likewise, using zonal statistics [77], the average values of the vegetation indices at the individual tree level were extracted using QGIS 3.28 software. This algorithm calculated the mean value of the pixels of the vegetation indices for the entities present in the layer of overlapping polygons (i.e., the buffer that represented the tree crowns).

For NDVI, the criterion with which to identify individual trees with signs of devitalization was that of values equal to or less than 0.4 [78]. For LCI, a criterion value of equal to or less than 0.09 was used to classify trees as stressed [79]. The function generated the resulting data in tabular form or as a vector layer file. This same process was used to extract the altitude in which each of the detected trees was located using the DTM layer generated in the photogrammetric process.

2.7. Climate Change Time-Series Analyses

In order to explore if the studied year (2022) was atypical or not in the context of a larger time period and to demonstrate the extent of climatic changes that have occurred in recent decades, we examined the mean annual temperature (MAT) and April temperature of the altitudinal transect studied. Additionally, we analyzed the April temperature of the xeric limit (low altitude) for each year from 1960 to 2022. Furthermore, in order to characterize how much the level of drought had increased in the study area, we analyzed the Palmer Drought Severity Index (PDSI), which is a well-known meteorological drought index proposed by Palmer [80] that encompass the balance between temperature and precipitation, as well as the soil water retention capacity. This index has been used to demonstrate the association between the occurrence of hotter droughts (induced by climatic change) with

the ongoing worldwide forest decline [14], as well as the association between the weakness of Mexican conifer trees due to drought stress and incidence of bark beetle outbreaks [81]. The data for these analyses were obtained from the TerraClimate website [82]. We obtained MAT, monthly April temperatures, and PDSI values for each year from TerraClimate pixels, which represent the climate along the altitudinal transect. We used three pixels that encompassed our examined elevation range: an upper altitudinal pixel covering altitudes from 4040 to 3900 m of elevation, an intermediate altitude pixel from 3900 to 3550 m, and a low altitudinal pixel covering elevations from 3550 to 3300 m. These three values were averaged to represent the whole transect, and the lower elevation pixel was also examined separately as proxy to represent the xeric limit of the *P. hartwegii* elevational range distribution.

2.8. Statistical Analysis

To detect possible differences in the canopy vigor of *P. hartwegii* trees in terms of the vegetation indices (NDVI and LCI) along the altitudinal gradient, a one-way analysis of variance (ANOVA) was performed using the statistical software R (version 4.1.2, Vienna, Austria) [83]. Subsequently, a post hoc analysis was performed to determine the significant differences between each altitudinal range (i.e., 3300, 3400, 3500, 3600, 3700, 3800, 3900, and 4000 m). The means were compared using Tukey's test with a *p*-value of ≤ 0.05 .

The workflow of the approach proposed in this study is shown in Figure 4.

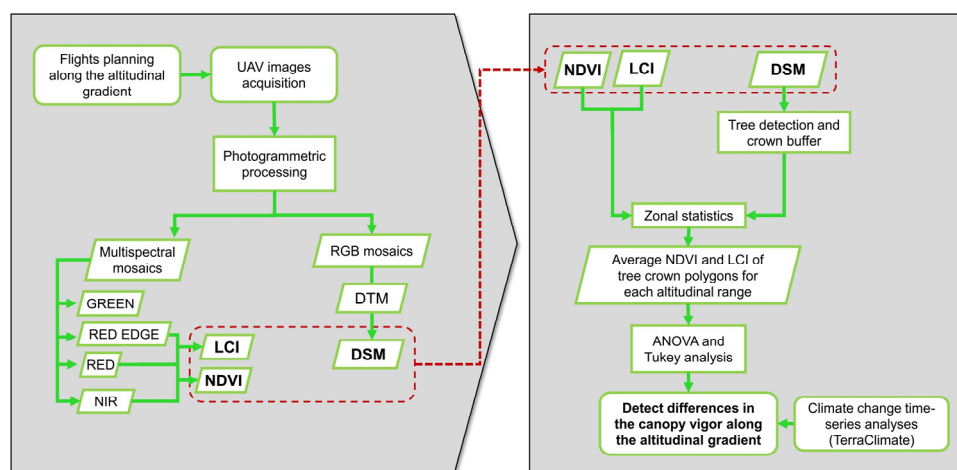


Figure 4. Flow diagram of the proposed approach. LCI: leaf chlorophyll index, NDVI: normalized difference vegetation index, DSM: digital surface model, DTM: digital terrain model.

3. Results

A total of 16,734 images were acquired using the P4M sensors, which encompassed blue, green, red, red-edge, and near-infrared bands. Figure 5 shows the multispectral orthomosaic digital terrain model, as well as maps of slope and aspect variables derived from the photogrammetric process using ODM and QGIS 3.28. Together with the four flight missions, it was possible to cover a horizontal distance of 4343 m along the altitudinal gradient where *P. hartwegii* is distributed, ranging from 3300 to 4040 m. Consequently, the overflowed coverage area was 90 ha, with a spatial resolution or ground sampling distance (GSD) of 10 cm [84].

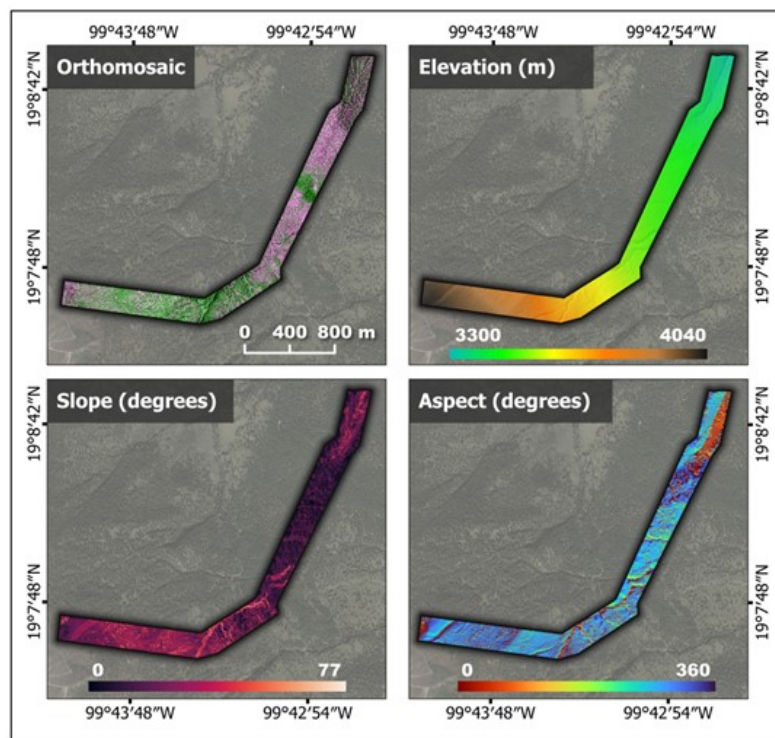


Figure 5. Multispectral orthomosaic digital terrain model (DTM): maps of slope and aspect variables derived from the UAV flight.

Using the Tree Density Calculator developed as plugin to QGIS, 4861 *P. hartwegii* trees were detected. Figure 6 shows an overview of all the detected trees (yellow dots) along the altitudinal gradient. It is important to note that, to focus the analysis on forests dominated by this tree species, a visual interpretation was used to exclude areas with apparent land use changes and where *P. hartwegii* occurred at low densities and coexisted with other species. Likewise, an example of three zones along the altitudinal gradient is shown (Figure 6a–c). The detected trees were adults (upper stratum) of variable phenotypic formation and open canopies, which allowed for the efficient detection of trees in this study.

Regarding the estimations of vegetation indices, Figure 7 shows the NDVI and LCI maps along the altitudinal gradient where *P. hartwegii* was distributed. The values of the vegetation indices that referred to the *P. hartwegii* tree crowns were visually recognizable in the zones with values close to 1 (i.e., green tones for NDVI and yellow tones for LCI, Figure 7). The difference was evident between tree canopies and surfaces corresponding to bare soil or shrub and herbaceous vegetation, with values close to −1 (red tones for NDVI and violet tones for LCI). However, it was possible to recognize the differences in the values of both indices in the crowns of *P. hartwegii* trees along the altitudinal gradient, which was likely attributable to different stress levels. As a result, Figure 7 demonstrates that each index displayed a distinct histogram shape. The varying shapes of the histograms indicate the diverse sensitivity of the indices in distinguishing between categories of disturbance and/or forest productivity [27].

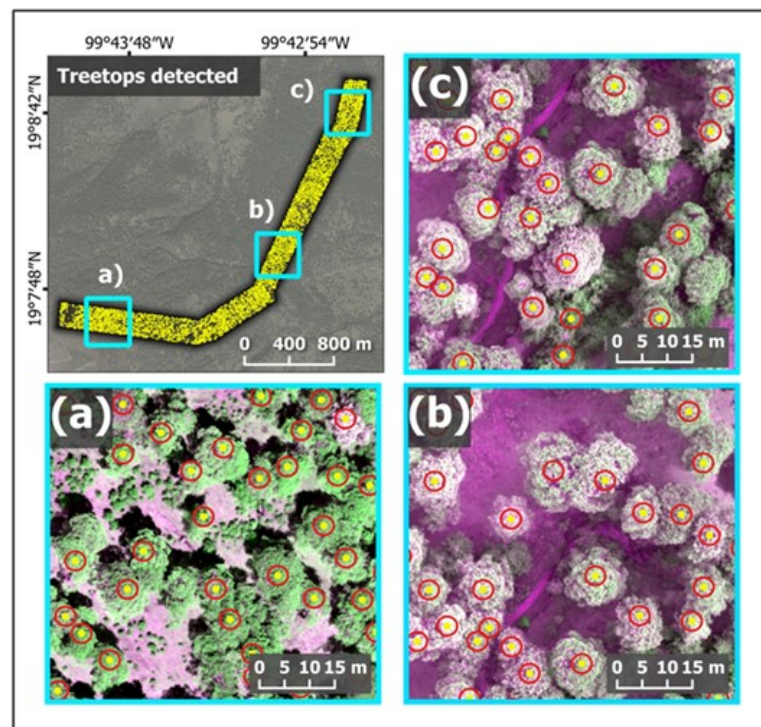


Figure 6. Detection and zone of influence (Buffer) of individual tree crowns derived from the Tree Density Calculator. (a–c) correspond to approaches at different altitudes along the gradient where *Pinus hartwegii* was distributed. The yellow dots indicate the treetops detected and the red circles indicate the zone of influence for each tree crown.

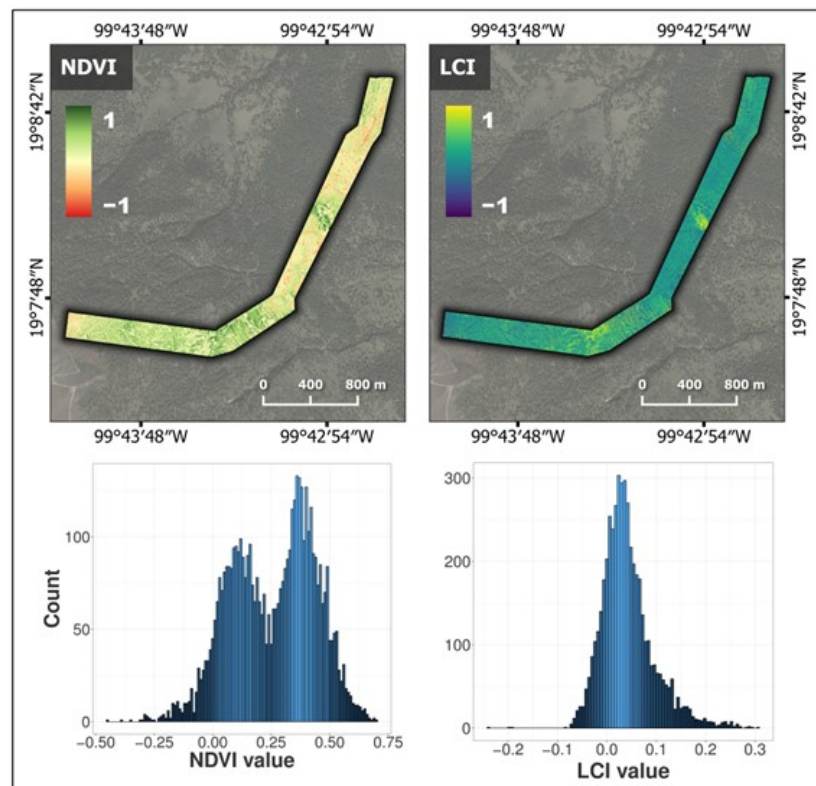


Figure 7. Maps of the normalized difference vegetation index (NDVI) and leaf chlorophyll index (LCI) along the altitudinal gradient, and frequency histogram for the detected tree crowns of *Pinus hartwegii*.

Table 1 provides the descriptive statistics for the indices' values corresponding to the crowns of the detected *P. hartwegii* trees. In terms of the distribution of vegetation indices, the NDVI exhibited an average of 0.25. Similarly, 25% of the trees displayed values ranging between 0.7 and 0.4. Conversely, the LCI values were distributed within a narrower range compared to the NDVI; the maximum value of this index was 0.31, the minimum was −0.24, and the average was 0.04. This lower range of LCI values could be attributed to the heightened stress levels experienced by the *P. hartwegii* trees. Figure 7 visually emphasizes the photosynthetic activity and varying vitality of the vegetation across the altitudinal gradient.

Table 1. Descriptive statistics of vegetation indices of the detected *Pinus hartwegii* tree crowns.

Descriptive Measure	NDVI	LCI
Minimum	−0.45	−0.24
First quartile	0.11	0.01
Median	0.28	0.03
Mean	0.26	0.04
Third quartile	0.40	0.07
Maximum	0.70	0.31
Standard deviation	0.18	0.05

NDVI, normalized difference vegetation index; LCI, leaf chlorophyll index.

The above analysis resulted in the formation of a database, which allowed for the visualization of the behavior of NDVI and LCI along the altitudinal gradient of the 4861 detected *P. hartwegii* trees (Figure 8). The lower altitude (i.e., 3300 m) populations exhibited higher stress conditions, represented by lower values of NDVI (mean ± standard error (SE): 0.048 ± 0.0054) and LCI (mean ± SE: 0.01 ± 0.001). These values increased nine to ten-fold in the intermediate altitude (i.e., 3600 m) populations, indicating higher tree vigor detected in terms of NDVI (mean ± SE: 0.44 ± 0.0050) and LCI (mean ± SE: 0.10 ± 0.003).

Subsequently, a one-way ANOVA was performed to analyze the effect of altitude on the vigor of *P. hartwegii* trees in terms of the NDVI and LCI vegetation indices. The ANOVA revealed a statistically significant difference in the mean values of NDVI and LCI between at least two altitudinal ranges [F (value of a test statistic) = 741.8; degrees of freedom (d.f.): 7, 4853; $p < 0.0001$ and $F = 396.4$, d.f.: 7, 4853; $p < 0.0001$, respectively]. A Tukey's HSD test was performed for multiple comparisons (28 possible combinations) of the means of the vegetation indices for each altitudinal range (Figure 8). It was found that the mean values of NDVI and LCI differed significantly in 27 and 24 combinations, respectively. The NDVI did not differ in the comparison of the altitudinal ranges: 3700 vs. 3800 m. The LCI did not differ in the comparisons of 3300 vs. 3400, 3500 vs. 3900, 3300 vs. 4000, and 3400 vs. 4000 m. The NDVI values presented their greatest difference between 3300 and 3600, followed by 3300 and 3700 m, while the altitudinal ranges with the greatest differences in LCI values were 3300 vs. 3600 and 3400 vs. 3600 m (see Figure S1 of the Supplementary Material).

Significantly devitalized trees were observed in all altitudinal gradients; however, the highest proportion of stressed trees was found at the xeric limit (from 3300 to 3400 m) of *P. hartwegii* (99% of devitalized trees; Figure 9). For NDVI, the stressed trees were considered to be those with values equal to or less than 0.4 [78]. For LCI, values equal to or less than 0.09 were used as the criterion for classifying trees as stressed [79]. It is important to note that, despite considering different criteria to define trees as devitalized in the NDVI and LCI, the percentage of devitalized trees in Figure 9 showed a high degree of similarity for both vegetation indices.

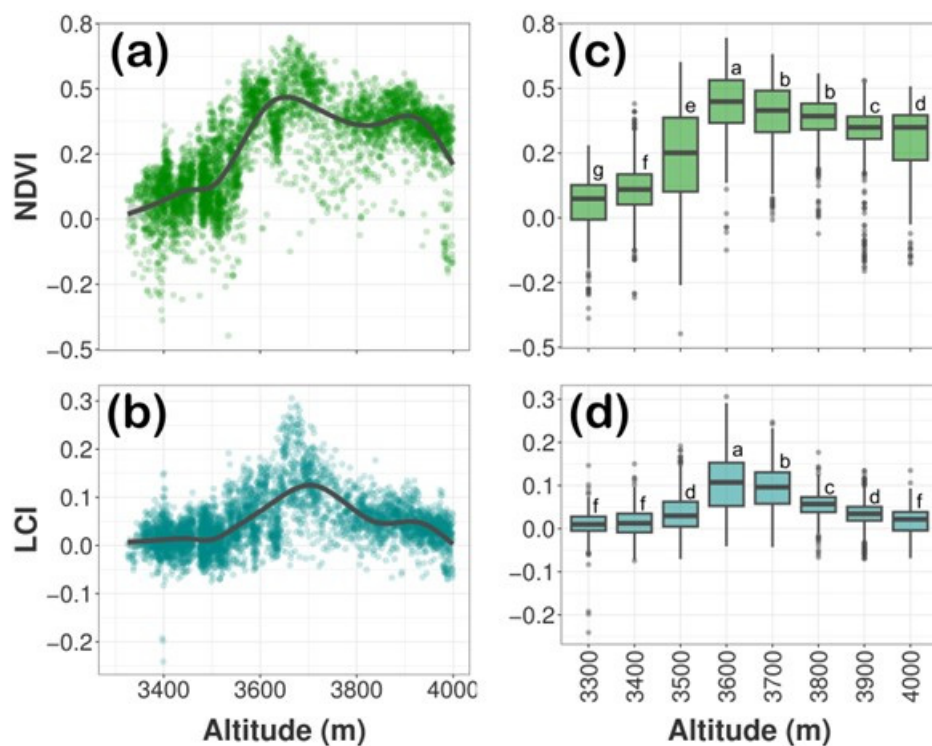


Figure 8. *Pinus hartwegii* crown vegetation index behavior along the altitudinal gradient. (a,b) indicate trend along altitudinal gradient for NDVI and LCI respectively (lines were smoothed using the ‘stat_smooth’ function of the ggplot2 package; method Z ‘gam’ in R). (c,d) correspond the boxplot summarizing the NDVI and LCI values in each of the eight altitudinal ranges. The line across the box corresponds to the median and the rectangle corresponds to the interquartile range. Boxes with the same letter do not differ significantly (multiple comparisons of means Tukey’s post hoc test, $p \leq 0.05$).

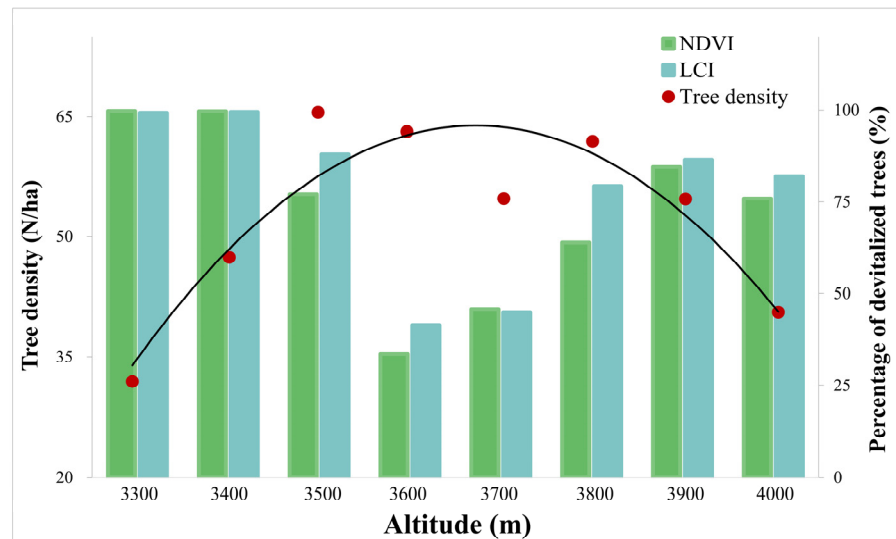


Figure 9. Density and percentage of significantly devitalized *Pinus hartwegii* trees ($NDVI \leq 0.4$; $LCI \leq 0.09$) along the altitudinal gradient.

The analysis of MAT and April temperature from the studied altitudinal transect and xeric limit for the period 1960–2022 revealed that the studied year (2022) was not atypical; it was in line with the longer-term trend of a steady increase in temperatures evident after 1980 (Figure 10a). Furthermore, the analysis of the climatic data of the average of three sites at contrasting altitudes (low, medium, and high altitude) (see Figure S2 of the Supplementary Material) revealed that the altitudinal transect has experienced in average a temperature

increase of 1.03°C when comparing the reference period 1961–1990 (average MAT: 8.95°C) against the decade preceding to our study (2011–2020; average MAT: 9.98°C). This phenomenon was experienced with greater intensity at the xeric limit of the transect (low altitude; increase of 1.4°C) when comparing the April temperature in the reference period 1961–1990 (mean: 12.17°C) with the decade prior to our study (2011–2020; mean: 13.57°C).

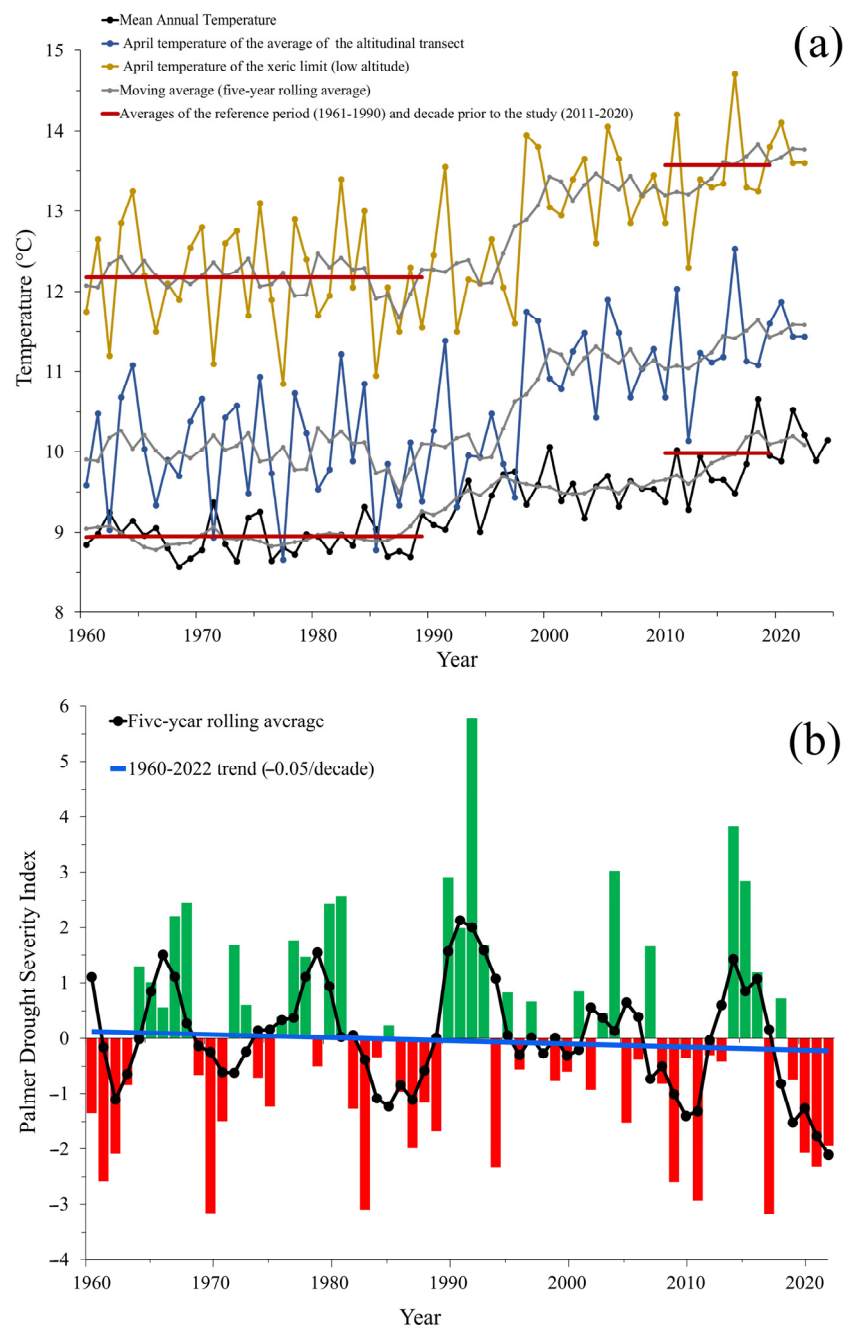


Figure 10. (a) Trend of the mean annual temperature (MAT, black line) and April temperature along the studied altitudinal transect (blue line) and April temperature only of the xeric limit (low altitude, yellow line) for the period 1960–2022. For MAT and April (blue line) temperature, each symbol represents the average across the upper, medium, and low elevation part of the studied transect for each year; however, for April, the temperature of the xeric limit only showed the temperature from the extreme lower altitude of the transect. (b) Annual values of the Palmer Drought Severity Index (PDSI) of the altitudinal transect (also averaged across upper, medium, and low altitudes of the transect) for the same period as above panel. The black line represents a five-year rolling-average, and blue line shows a linear regression to indicate the overall trend.

Figure 10b shows the PDSI trend along the altitudinal transect. Positive values represent wetter conditions, while negative values represent drier conditions. A value between -2 and -3 indicates moderate drought, while -3 to -4 represents severe drought. The trend from 1960 to 2020 indicates that drought in the study area has increased at a rate of 0.05 PDSI units per decade, with greater intensity in the last five years (solid lines in Figure 10b). This trend is slightly higher for the xeric limit of the transect (low altitude), at a rate of 0.06 PDSI units per decade (see Figure S3 of the Supplementary Material).

4. Discussion

The methodology used allowed for the detection, estimation, and analysis of two multispectral indices (NDVI and LCI) of *P. hartwegii* tree crowns at the individual level. The most notable aspect of this research was to determine that the lower limit of the altitudinal distribution of *P. hartwegii* presents higher levels of stress, evidenced by lower NDVI and LCI values (Figure 8). Likewise, the highest proportion of devitalized individuals ($>90\%$) was observed between 3300 and 3400 m (Figure 9). The average increase in MAT and April temperature along the studied altitudinal transect and xeric limit compared to the reference period of 1961–1990 was 1.03 and 1.4°C , respectively (Figure 10a). These temperature increases seem to be causing a devitalization effect on *P. hartwegii* populations, particularly pronounced at the lower distribution limit. This weakening effect was investigated by analyzing tree-ring variables of this species in the same region of the country, revealing a decrease in growth rate (less annual ring width) at the low altitudinal limit of *P. hartwegii* [85]. In addition, the PDSI analysis revealed an intensification of droughts in the study area. This index has proven instrumental in understanding how droughts are triggering amplified outbreaks of bark beetles in temperate forests in central Mexico [81]. Although stress conditions are characteristic of the distribution limits of each species [86], there was a notable difference between the responses of the species at the lower and upper limits. Mátyás et al. [87] stated that the most threatened forest communities are those found at the limits with lower moisture availability and a higher increase in temperatures, i.e., the lower altitudinal or xeric limit. The term xeric limit has been introduced to emphasize the role of the rapidly changing climate in shaping the altitudinally lower limits of species distribution [19–21,88].

If we consider that April is the warmest and driest month of the year in the studied region, it is reasonable to assume that the xeric limit was defined by the April climate to a large extent. Thus, an increase of $+1.4^{\circ}\text{C}$ in April temperature in the last decade is equivalent to a shifting upwards in altitude by 280 m of this xeric limit (considering a temperature lapse rate of approximately 0.5°C per each 100 m of altitudinal difference [13]). This likely indicates that the *P. hartwegii* populations present occupying elevations close to 3300 m altitude at Nevado de Toluca (notice the low NDVI values between 3300 and 3500 m in Figure 8) are the ones that will suffer the most due to increasing drought stress and will likely experience greater risks of bark beetle outbreak occurrences and tree dieback.

Our results are consistent with recent findings regarding the decrease in growth rates and loss of vigor in temperate forest tree species, especially at their xeric limit. For example, Ricker et al. [89] developed models that predicted a 10.6% decrease in the relative growth of *P. hartwegii* as a result of a 0.6°C temperature increase. Carrillo-Arizmendi et al. [85] analyzed the dendrochronological series of *P. hartwegii* and concluded that global warming appears to be the main driver of variation in the radial growth of this tree species, with warning signs were observed at the lower extreme of its distribution gradient. Low NDVI and LCI values at lower altitudes suggest a process of forest devitalization expressed as a decrease in photosynthetic activity. Increasingly intense and hotter droughts associated with the xeric limit [14] are causing physiological weakness in trees, promoting damage by pests and diseases and the eventual appearance of forest decline phenomena [90].

In this regard, Gómez-Pineda et al. [81] reported that 54% of the bark beetle outbreaks that attack *Pinus pseudostrobus* were found at the xeric limit of this important conifer species present in the TMVB. In a description of the recent altitudinal distribution pattern of *Dendroctonus adjunctus* (a species strongly associated with *P. hartwegii*) in forests of central

Mexico, it was observed that the area with the highest abundance of this insect was between 3400 and 3500 m, with a significant decrease towards the intermediate limit of distribution of *P. hartwegii*. Likewise, it was observed that the abundance of *Dendroctonus* spp. was variable and related to extreme drought events [91].

The distribution patterns of the devitalized trees found in the present study may also be related to the decline in the reproductive performance of this species with respect to an altitudinal gradient. For example, Tejeda-Landero et al. [92] evaluated the viability of *P. hartwegii* seeds at four altitudes (3400, 3600, 3800, and 4000 m) within the Cofre de Perote National Park, Veracruz, Mexico. The main results of this study showed that the highest values of seed viability occurred at the upper limits, in contrast to those of the lower altitude site. However, variations in these types of indicators have been found among different mountains. Alba-Landa et al. [93] compared the seed potential and efficiency of *P. hartwegii* populations in La Malinche National Park and Cofre de Perote National Park in Mexico, reporting higher efficiency percentages for La Malinche (75%) compared to Cofre de Perote (68%) and detecting development problems for the latter site. This suggests that the dynamics of forest decline have particular characteristics for each mountain system. Therefore, it is suggested that future research should conduct more flights in altitudinal transects and different orientations in various high mountain ecosystems throughout the country.

In contrast, the higher NDVI values and the lower proportion of devitalized trees at the upper limit of *P. hartwegii* distribution compared to those at the xeric limit suggest that the individuals were under conditions of lower stress. This supports Astudillo-Sánchez et al. [94] who reported that in the upper zones of altitudinal distribution, increased temperature in shaded and humid conditions may act to increase the number of individuals of *P. hartwegii*. Although *P. hartwegii* is a vulnerable species due to its extreme altitudinal distribution, the individuals present at the lower limit appear to suffer greater alterations due to climate change.

The results of the present study suggest that the studied *P. hartwegii* populations are already suffering the impacts of climate change. Castellanos-Acuña et al. [95] warned that by the 2050s, the mean temperature of the coldest month (a variable related to the genetic adaptation of tree species) will increase by 1.7 °C, and a shift towards drier conditions overall is predicted throughout Mexico. In support of this projection, Manzanilla-Quiñones et al. [96] reported an increase in mean annual temperature of between 0.7 and 2.1 °C and reductions of between 11.7 and 26.9% in the subalpine niche of *P. hartwegii*, with Nevado de Toluca and Pico de Orizaba reported as the sites most susceptible to climate change. Alfaro-Ramírez et al. [6] emphasized that the area of environmental suitability for *P. hartwegii* will be reduced by up to 70% as a result of the increase in temperature.

The above findings seem to coincide with Millar and Stephenson [97], who provided evidence that the increasingly frequent extreme droughts have been accompanied by records of decreasing NDVI values, an increase in the area affected by bark beetles, and a greater forest mortality in temperate forests worldwide. A clear example of this process is the loss of climatically favorable habitats for conifers in the Sierra Nevada in California, which has caused massive tree mortality followed by catastrophic wildfires due to a 1.2 °C increase in mean annual temperature since the 1930s [98].

The ranges in which the NDVI and LCI of *P. hartwegii* reported in the present study are distributed support that found in other studies. Among those studies that utilized the NDVI, Dash et al. [28] simulated a disease outbreak and treated trees selected from a *Pinus radiata* plantation with herbicide. The NDVI proved to be the most sensitive vegetation index to physiological changes in leaf pigments, even during the early stages of tree stress. These findings are consistent with our results, as the NDVI was more sensitive than LCI in terms of detecting differences between stress levels of the *P. hartwegii* trees (Figure 8). Figure 7 displays distinct histogram shapes for each index, indicating the varying sensitivity of these indices in distinguishing between different categories of disturbance forest productivity. According to Minařík and Langhammer [99], this underscores the superior capability of NDVI as the most effective index in this regard. This is based on the

assumption that high NDVI values in healthy foliage are associated with photosynthetic activity [100,101] due to the contrast in low leaf reflectance in the red band that occurs with increased chlorophyll absorption and high infrared reflection within the spongy mesophyll layer [102]. NDVI values decrease with foliage senescence, which is associated with higher reflectance in the red band [103,104]. On the other hand, Datt [38] demonstrated that the LCI presents a higher sensitivity to chlorophyll content, concluded that it was the best-performing vegetation index, and proposed its use as a new index for the remote estimation of chlorophyll content in trees of the genus *Eucalyptus*. Likewise, Eitel et al. [35] documented that red-edge information improved early detection of stress (changes in chlorophyll content) in a stone pine–juniper forest in central New Mexico. The authors concluded that red-edge information has the potential to significantly improve forest stress monitoring, warranting further research with this technology in forested ecosystems with symptoms of forest decline possibly associated with climate change [34].

Although the NDVI and LCI vegetation indices employed in our study have demonstrated ample sensitivity for distinguishing tree devitalization levels along the altitudinal gradient, we acknowledge the limitations of our research due to the absence of ground estimations of tree vigor or chlorophyll content (or so) data to compare our findings. For example, we believe that measuring the chlorophyll content of coniferous needles would provide additional insights into the influence of climatic factors on plant growth and phenological status. Additionally, for further researches the possibility of conducting phenology and xylogenetic studies to enhance the precision of dendroclimatic proxies and its relationship with the vegetation indices computed with UAV multispectral images should not be dismissed.

The techniques and UAV used in this study made it possible to generate multispectral orthomosaic and maps of microtopographic variables (i.e., digital terrain model, slope map, and aspect map) of the study area. A total of 90 ha was covered along the altitudinal gradient where *P. hartwegii* was distributed (Figure 1). Although recent literature has reported an exponential interest in UAV applications in forestry studies [105], the flight area reported in previous research has not exceeded 30 ha [45]. In addition, the flights tended to be concentrated on flat areas with regular shapes (most frequently in commercial forestry plantations). In the present study, the high degree of technical difficulty involved in overflying 4.3 km longitudinally along an altitudinal gradient in a high mountain ecosystem is notable (Figure 5). This indicates that short-range remote sensing performed using UAV represents a promising alternative to complement the information gathered in the field [61,106].

The methodology used in this study allowed for the detection of 4861 *P. hartwegii* trees along the studied altitudinal gradient. Although it was beyond the scope of this research to evaluate the detection capacity of the applied algorithms by validating them with field sampling, there is previous knowledge of the high efficiency of tree detection using information derived from UAV and specialized algorithms. For example, Gallardo-Salazar and Pompa-García [71] reported 95% detection effectiveness in a clonal orchard of *Pinus arizonica*. Mohan et al. [70] documented the entire public-focused workflow, starting in the area of UAV photogrammetry and achieving detection of 80% of the trees in a *Pinus elliottii* plantation. Gonroudobou et al. [107] achieved a maximum tree detection rate of 90.8% in a mountain ecosystem dominated by *Abies mariesiesii*. The methods used to detect and geolocate trees from information provided by UAV and photogrammetry are therefore considered suitable and can be recommended for coniferous forests, especially due to the shape of the dominant tree crowns, which can facilitate their detection [73]. However, it is important to highlight that tree detection using these technologies may lead to an underestimation of the actual density of trees present in stands, as only the upper stratum (dominant trees) can be reliably detected. Combining multispectral information with airborne LiDAR technology (active sensor) could be of great importance for detailed monitoring across multiple strata of the ecosystem to better understand the forest decline related to climate change [108].

5. Conclusions

Symptoms of forest decline were detected in *Pinus hartwegii* populations in the form of low values of the normalized difference vegetation index (NDVI) and leaf chlorophyll index (LCI). The research hypothesis was therefore confirmed: NDVI and LCI data exhibited heterogeneous behavior along the altitudinal gradient, with a higher proportion of devitalized individuals found at the xeric limit (lower altitudinal distribution range). Individuals located in the intermediate part of the altitudinal distribution showed spectral characteristics associated with conditions of higher plant vigor, which was consistent with the values reported in the literature for *P. hartwegii* and other conifer species.

This study conducted along the altitudinal gradient allowed us to demonstrate that UAV are capable of providing high-quality information, with an adequate spatial and spectral resolution to analyze the stress/vigor conditions of *P. hartwegii* populations distributed within the Nevado de Toluca Flora and Fauna Protection Area and a single-tree resolution. This contributes to knowledge, furthers our understanding of how this species responds to global warming, and highlights a clear threat to the persistence of these forests and the ecosystem services they provide. The results of the present study elucidated the factors that influence the vigor of *P. hartwegii* populations, which are expected to provide a theoretical basis for decision-making that will contribute to the development of forest management alternatives and targeted conservation practices to increase resilience and adaptation in the high mountain ecosystems.

Supplementary Materials: The following supporting information can be downloaded at: <https://www.mdpi.com/article/10.3390/f14061176/s1>. Table S1: Spectral information of the bands for the DJI Phantom 4 Multispectral UAV (P4M), Table S2: Characteristics of the flight missions conducted along the altitudinal gradient where *Pinus hartwegii* is distributed, Figure S1: Difference of the vegetation index means, Figure S2: Trend of the Mean Annual Temperatures (MAT) from the study area, Figure S3: Annual values of the Palmer Drought Severity Index (PDSI) of the xeric limit of the transect (low altitude).

Author Contributions: C.S.-R. and J.L.G.-S. planned and designed the research; J.L.G.-S. and C.S.-R. led the writing of the manuscript. J.L.G.-S. contributed to data analysis and R.A.L.-C., L.L.-T., A.R.E.-A. and A.B.-G. determined the statistical analyses and provided important suggestions during the development of the project and for the data discussion. All authors have read and agreed to the published version of the manuscript.

Funding: Financial support was provided to C.S.-R. by The Monarch Butterfly Fund (Madison, WI, USA) and Coordinación de la Investigación Científica of the Universidad Michoacana de San Nicolás de Hidalgo (6790204), to R.L.-C. by the PAPIIT-UNAM program (IG 200221) of UNAM, and a Mexican National Council of Science and Technology (CONACyT) graduate studies fellowship was provided to J.L.G.-S. (815176).

Data Availability Statement: The data presented in this study are available from the corresponding author upon request.

Acknowledgments: We would like to thank Mario Fermin Castañeda-Rojas and Dulce María Avendaño-Hernández of the Mexican Federal Natural Forest Commission of Natural Protected Areas (CONANP by its Spanish acronym) for providing the facilities used in this study, and the former (Bonifacio González-Gomora) and present (Jose Luis Malvais-Ríos) presidents of the Consejo de Bienes Comunales for providing access permits and continued extraordinary support. We would also like to thank the staff of the forest technicians team (Josué Eduardo Carmona-López, Pablo Trinidad Rosas-Quiñones, Víctor Mendoza-Zarza, Ángel Rosas-Villegas, and Eduardo Bonifacio Mendoza-Zarza) and others of Calimaya Community, Estado de México for help and guidance in the field. Without their help, this study would not have been possible. Cielito Drone Enterprise company (México city), an authorized distributor of DJI Enterprise (China), provided (under an informal no-profit loan agreement) a Phantom 4 Multispectral (P4M) quadcopter. Keith MacMillan assisted with the English language revision of the manuscript.

Conflicts of Interest: The authors declare no conflict of interest.

References

1. Lauer, W. The Altitudinal Belts of the Vegetation in the Central Mexican Highlands and Their Climatic Conditions. *Arct. Alp. Res.* **1973**, *5*, A99–A113. [[CrossRef](#)]
2. Lauer, W.; Klaus, D. Geoecological Investigations on the Timberline of Pico De Orizaba, Mexico. *Arct. Alp. Res.* **1975**, *7*, 315–330. [[CrossRef](#)]
3. Viveros-Viveros, H.; Sáenz-Romero, C.; Vargas-Hernández, J.J.; López-Upton, J.; Ramírez-Valverde, G.; Santacruz-Varela, A. Altitudinal Genetic Variation in *Pinus hartwegii* Lindl. I: Height Growth, Shoot Phenology, and Frost Damage in Seedlings. *For. Ecol. Manag.* **2009**, *257*, 836–842. [[CrossRef](#)]
4. Viveros-Viveros, H.; Sáenz-Romero, C.; López-Upton, J.; Vargas-Hernández, J.J. Growth and Frost Damage Variation among *Pinus pseudostrobus*, *P. montezumae* and *P. hartwegii* Tested in Michoacán, México. *For. Ecol. Manag.* **2007**, *253*, 81–88. [[CrossRef](#)]
5. Iglesias, L.G.; Solís-Ramos, L.Y.; Viveros-Viveros, H. Variación Morfométrica En Dos Poblaciones Naturales de *Pinus hartwegii* Lindl. Del Estado de Veracruz. *Phyton* **2012**, *81*, 239–246.
6. Alfaro-Ramírez, F.U.; Ramírez-Albores, J.E.; Vargas-Hernández, J.J.; Franco-Maass, S.; Pérez-Suárez, M. Potential Reduction of Hartweg’s Pine (*Pinus hartwegii* Lindl.) Geographic Distribution. *PLoS ONE* **2020**, *15*, e0229178. [[CrossRef](#)]
7. Malhi, Y.; Franklin, J.; Seddon, N.; Solan, M.; Turner, M.G.; Field, C.B.; Knowlton, N. Climate Change and Ecosystems: Threats, Opportunities and Solutions. *Philos. Trans. R. Soc. B Biol. Sci.* **2020**, *375*, 20190104. [[CrossRef](#)]
8. Ripple, W.J.; Wolf, C.; Newsome, T.M.; Barnard, P.; Moomaw, W.R. World Scientists’ Warning of a Climate Emergency. *Bioscience* **2020**, *70*, 8–12. [[CrossRef](#)]
9. Beniston, M. Climatic Change in Mountain Regions: A Review of Possible Impacts. *Clim. Change* **2003**, *59*, 5–31. [[CrossRef](#)]
10. Fort, M. Impact of Climate Change on Mountain Environment Dynamics: An Introduction. *J. Alp. Res.* **2015**, *103*, 2–7. [[CrossRef](#)]
11. Sáenz-Romero, C.; Mendoza-Maya, E.; Gómez-Pineda, E.; Blanco-García, A.; Endara-Agramont, A.R.; Lindig-Cisneros, R.; López-Upton, J.; Trejo-Ramírez, O.; Wehenkel, C.; Cibrián-Tovar, D.; et al. Recent Evidence of Mexican Temperate Forest Decline and the Need for Ex Situ Conservation, Assisted Migration, and Translocation of Species Ensembles as Adaptive Management to Face Projected Climatic Change Impacts in a Megadiverse Country. *Can. J. For. Res.* **2020**, *50*, 843–854. [[CrossRef](#)]
12. Liu, L.; Wang, Z.; Wang, Y.; Zhang, Y.; Shen, J.; Qin, D.; Li, S. Trade-off Analyses of Multiple Mountain Ecosystem Services along Elevation, Vegetation Cover and Precipitation Gradients: A Case Study in the Taihang Mountains. *Ecol. Indic.* **2019**, *103*, 94–104. [[CrossRef](#)]
13. Sáenz-Romero, C.; Rehfeldt, G.E.; Crookston, N.L.; Duval, P.; St-Amant, R.; Beaulieu, J.; Richardson, B.A. Spline Models of Contemporary, 2030, 2060 and 2090 Climates for Mexico and Their Use in Understanding Climate-Change Impacts on the Vegetation. *Clim. Change* **2010**, *102*, 595–623. [[CrossRef](#)]
14. Hammond, W.M.; Williams, A.P.; Abatzoglou, J.T.; Adams, H.D.; Klein, T.; López, R.; Sáenz-Romero, C.; Hartmann, H.; Breshears, D.D.; Allen, C.D. Global Field Observations of Tree Die-off Reveal Hotter-Drought Fingerprint for Earth’s Forests. *Nat. Commun.* **2022**, *13*, 1761. [[CrossRef](#)]
15. Forzieri, G.; Dakos, V.; McDowell, N.G.; Ramdane, A.; Cescatti, A. Emerging Signals of Declining Forest Resilience under Climate Change. *Nature* **2022**, *608*, 534–539. [[CrossRef](#)]
16. Stevens, M. 102 Million Dead California Trees ‘Unprecedented in Our Modern History’, Officials Say. Los Angeles Times. 2016. Available online: <https://www.latimes.com/local/lanow/la-me-dead-trees-20161118-story.html> (accessed on 3 April 2023).
17. Jay, L.; Josue, M.-A.; John, D.; Kathleen, S. Lessons from California’s 2012–2016 Drought. *J. Water Resour. Plan Manag.* **2018**, *144*, 04018067. [[CrossRef](#)]
18. Allen, C.D.; Macalady, A.K.; Chenchouni, H.; Bachelet, D.; McDowell, N.; Vennetier, M.; Kitzberger, T.; Rigling, A.; Breshears, D.D.; Hogg, E.H.T.; et al. A Global Overview of Drought and Heat-Induced Tree Mortality Reveals Emerging Climate Change Risks for Forests. *For. Ecol. Manag.* **2010**, *259*, 660–684. [[CrossRef](#)]
19. Mátyás, C. Forecasts Needed for Retreating Forests. *Nature* **2010**, *464*, 1271. [[CrossRef](#)]
20. Czucz, B.; Gálhidy, L.; Mátyás, C. Present and Forecasted Xeric Climatic Limits of Beech and Sessile Oak Distribution at Low Altitudes in Central Europe. *Ann. For. Sci.* **2011**, *68*, 99–108. [[CrossRef](#)]
21. Stojanović, D.B.; Kržić, A.; Matović, B.; Orlović, S.; Duputie, A.; Djurdjević, V.; Galić, Z.; Stojnić, S. Prediction of the European Beech (*Fagus Sylvatica* L.) Xeric Limit Using a Regional Climate Model: An Example from Southeast Europe. *Agric. For. Meteorol.* **2013**, *176*, 94–103. [[CrossRef](#)]
22. Allen, C.D.; Breshears, D.D.; McDowell, N.G. On Underestimation of Global Vulnerability to Tree Mortality and Forest Die-off from Hotter Drought in the Anthropocene. *Ecosphere* **2015**, *6*, 1–55. [[CrossRef](#)]
23. Huang, C.; Anderegg, W.R.L.; Asner, G.P. Remote Sensing of Forest Die-off in the Anthropocene: From Plant Ecophysiology to Canopy Structure. *Remote Sens. Environ.* **2019**, *231*, 111233. [[CrossRef](#)]
24. Gallardo-Salazar, J.L.; Sáenz-Romero, C.; Lindig-Cisneros, R.; López-Toledo, L.; Blanco-García, J.A.; Endara-Agramont, Á.R. Three Decades of Remote Sensing Analysis of Forest Decline Related to Climate Change: A Bibliometric Study. *Cuad. Investig. Geográfica* **2023**. [[CrossRef](#)]
25. Paneque-Gálvez, J.; McCall, M.; Napoletano, B.; Wich, S.; Koh, L. Small Drones for Community-Based Forest Monitoring: An Assessment of Their Feasibility and Potential in Tropical Areas. *Forests* **2014**, *5*, 1481–1507. [[CrossRef](#)]
26. Torresan, C.; Berton, A.; Carotenuto, F.; Di Gennaro, S.F.; Gioli, B.; Matese, A.; Miglietta, F.; Vagnoli, C.; Zaldei, A.; Wallace, L. Forestry Applications of UAVs in Europe: A Review. *Int. J. Remote Sens.* **2017**, *38*, 2427–2447. [[CrossRef](#)]

27. Gallardo-Salazar, J.L.; Carrillo-Aguilar, D.M.; Pompa-García, M.; Aguirre-Salado, C.A. Multispectral Indices and Individual-Tree Level Attributes Explain Forest Productivity in a Pine Clonal Orchard of Northern Mexico. *Geocarto Int.* **2021**, *37*, 4441–4453. [[CrossRef](#)]
28. Dash, J.P.; Watt, M.S.; Pearse, G.D.; Heaphy, M.; Dungey, H.S. Assessing Very High Resolution UAV Imagery for Monitoring Forest Health during a Simulated Disease Outbreak. *ISPRS J. Photogramm. Remote Sens.* **2017**, *131*, 1–14. [[CrossRef](#)]
29. Näsi, R.; Honkavaara, E.; Lyytikäinen-Saarenmaa, P.; Blomqvist, M.; Litkey, P.; Hakala, T.; Viljanen, N.; Kantola, T.; Tanhuanpää, T.; Holopainen, M. Using UAV-Based Photogrammetry and Hyperspectral Imaging for Mapping Bark Beetle Damage at Tree-Level. *Remote Sens.* **2015**, *7*, 15467–15493. [[CrossRef](#)]
30. Brovkina, O.; Cienciala, E.; Surový, P.; Janata, P. Unmanned Aerial Vehicles (UAV) for Assessment of Qualitative Classification of Norway Spruce in Temperate Forest Stands. *Geo-Spat. Inf. Sci.* **2018**, *21*, 12–20. [[CrossRef](#)]
31. Lin, Q.; Huang, H.; Wang, J.; Huang, K.; Liu, Y. Detection of Pine Shoot Beetle (PSB) Stress on Pine Forests at Individual Tree Level Using UAV-Based Hyperspectral Imagery and Lidar. *Remote Sens.* **2019**, *11*, 2540. [[CrossRef](#)]
32. De Castro, A.I.; Shi, Y.; Maja, J.M.; Peña, J.M. UAVs for Vegetation Monitoring: Overview and Recent Scientific Contributions. *Remote Sens.* **2021**, *13*, 2139. [[CrossRef](#)]
33. Kopačková-Strnadová, V.; Koucká, L.; Jelének, J.; Lhotáková, Z.; Oulehle, F. Canopy Top, Height and Photosynthetic Pigment Estimation Using Parrot Sequoia Multispectral Imagery and the Unmanned Aerial Vehicle (UAV). *Remote Sens.* **2021**, *13*, 705. [[CrossRef](#)]
34. Ecke, S.; Dempewolf, J.; Frey, J.; Schwaller, A.; Endres, E.; Klemmt, H.-J.; Tiede, D.; Seifert, T. UAV-Based Forest Health Monitoring: A Systematic Review. *Remote Sens.* **2022**, *14*, 3205. [[CrossRef](#)]
35. Eitel, J.U.H.; Vierling, L.A.; Litvak, M.E.; Long, D.S.; Schulthess, U.; Ager, A.A.; Krofcheck, D.J.; Stoscheck, L. Broadband, Red-Edge Information from Satellites Improves Early Stress Detection in a New Mexico Conifer Woodland. *Remote Sens. Environ.* **2011**, *115*, 3640–3646. [[CrossRef](#)]
36. Zarco-Tejada, P.J.; Camino, C.; Beck, P.S.A.; Calderon, R.; Hornero, A.; Hernández-Clemente, R.; Kattenborn, T.; Montes-Borrego, M.; Susca, L.; Morelli, M.; et al. Previsual Symptoms of *Xylella Fastidiosa* Infection Revealed in Spectral Plant-Trait Alterations. *Nat. Plants* **2018**, *4*, 432–439. [[CrossRef](#)]
37. Huang, S.; Tang, L.; Hupy, J.P.; Wang, Y.; Shao, G. A Commentary Review on the Use of Normalized Difference Vegetation Index (NDVI) in the Era of Popular Remote Sensing. *J. For. Res.* **2021**, *32*, 1–6. [[CrossRef](#)]
38. Datt, B. A New Reflectance Index for Remote Sensing of Chlorophyll Content in Higher Plants: Tests Using Eucalyptus Leaves. *J. Plant Physiol.* **1999**, *154*, 30–36. [[CrossRef](#)]
39. Mejía Canales, A.; Franco-Maass, S.; Endara Agramont, A.R.; Ávila Akerberg, V. Caracterización Del Sotobosque En Bosques Densos de Pino y Oyamel En El Nevado de Toluca, México. *Madera Bosques* **2018**, *24*. [[CrossRef](#)]
40. Chávez-Aguilar, G.; Campos-Ángeles, G.V.; Pérez-Suárez, M. Estructura y Composición Del Bosque de *Pinus hartwegii* Lindl. En Su Distribución Altitudinal En El Nevado de Toluca. *Rev. Mex. Cienc. For.* **2022**, *13*, 54–76. [[CrossRef](#)]
41. Alfaro-Ramírez, F.U.; Arredondo-Moreno, J.T.; Pérez-Suárez, M.; Endara-Agramont, Á.R. *Pinus hartwegii* Lindl. Treeline Ecotone: Structure and Altitudinal Limits at Nevado de Toluca, Mexico. *Rev. Chapingo Ser. Cienc. For. Ambiente* **2017**, *23*, 261–273. [[CrossRef](#)]
42. Pérez-Suárez, M.; Ramírez-Albores, J.E.; Vargas-Hernández, J.J.; Alfaro-Ramírez, F.U. A Review of the Knowledge of Hartweg's Pine (*Pinus hartwegii* Lindl.): Current Situation and the Need for Improved Future Projections. *Trees* **2022**, *36*, 25–37. [[CrossRef](#)]
43. Gómez-Pineda, E.; Sáenz-Romero, C.; Ortega-Rodríguez, J.M.; Blanco-García, A.; Madrigal-Sánchez, X.; Lindig-Cisneros, R.; Lopez-Toledo, L.; Pedraza-Santos, M.E.; Rehfeldt, G.E. Suitable Climatic Habitat Changes for Mexican Conifers along Altitudinal Gradients under Climatic Change Scenarios. *Ecol. Appl.* **2020**, *30*, e02041. [[CrossRef](#)]
44. Loya-Rebollar, E.; Sáenz-Romero, C.; Lindig-Cisneros, R.A.; Lobit, P.; Villegas-Moreno, J.A.; Sánchez-Vargas, N.M. Clinal Variation in *Pinus hartwegii* Populations and Its Application for Adaptation to Climate Change. *Silvae Genet.* **2013**, *62*, 86–95. [[CrossRef](#)]
45. Gallardo-Salazar, J.L.; Pompa-García, M.; Aguirre-Salado, C.; López-Serrano, P.; Meléndez-Soto, A. Drones: Technology with a Promising Future in Forest Management. *Rev. Mex. For. Cienc.* **2020**, *11*. [[CrossRef](#)]
46. CONANP Programa de Manejo Área de Protección de Flora y Fauna Nevado de Toluca. Available online: https://simec.conanp.gob.mx/pdf_libro_pm/104_libro_pm.pdf (accessed on 2 April 2022).
47. Tapia-Vázquez, I.; Sánchez-Cruz, R.; Arroyo-Domínguez, M.; Lira-Ruan, V.; Sánchez-Reyes, A.; del Rayo Sánchez-Carbente, M.; Padilla-Chacón, D.; Batista-García, R.A.; Folch-Mallol, J.L. Isolation and Characterization of Psychrophilic and Psychrotolerant Plant-Growth Promoting Microorganisms from a High-Altitude Volcano Crater in Mexico. *Microbiol. Res.* **2020**, *232*, 126394. [[CrossRef](#)]
48. INEGI Cartografía Edafológica Temática, Escala 1:250,000. Available online: <https://www.inegi.org.mx/temas/edafologia/> (accessed on 3 April 2023).
49. Carlón Allende, T.; Villanueva Díaz, J.; Soto Castro, G.; Mendoza, M.E.; Macías, J.L. Tree Rings as Indicators of Climatic Variation in the Trans-Mexican Volcanic Belt, Central Mexico. *Ecol. Indic.* **2021**, *120*, 106920. [[CrossRef](#)]
50. Bravo-Espinosa, M.; Mendoza, M.E.; Medina-Orozco, L.; Prat, C.; García-Oliva, F.; López-Granados, E. Runoff, Soil Loss, and Nutrient Depletion under Traditional and Alternative Cropping Systems in the Transmexican Volcanic Belt, Central Mexico. *Land Degrad. Dev.* **2009**, *20*, 640–653. [[CrossRef](#)]

51. Cruzado-Vargas, A.L.; Blanco-García, A.; Lindig-Cisneros, R.; Gómez-Romero, M.; Lopez-Toledo, L.; de la Barrera, E.; Sáenz-Romero, C. Reciprocal Common Garden Altitudinal Transplants Reveal Potential Negative Impacts of Climate Change on Abies Religiosa Populations in the Monarch Butterfly Biosphere Reserve Overwintering Sites. *Forests* **2021**, *12*, 69. [CrossRef]
52. Villers-Ruiz, L.; Castañeda-Aguado, D. Species and Plant Community Reorganization in the Trans-Mexican Volcanic Belt under Climate Change Conditions. *J. Mt. Sci.* **2013**, *10*, 923–931. [CrossRef]
53. P4 Multispectral Specs. Available online: <https://www.dji.com/mx/p4-multispectral/specs> (accessed on 3 April 2023).
54. Lu, H.; Fan, T.; Ghimire, P.; Deng, L. Experimental Evaluation and Consistency Comparison of UAV Multispectral Minisensors. *Remote Sens.* **2020**, *12*, 2542. [CrossRef]
55. Syetiawan, A.; Gularso, H.; Kusnadi, G.I.; Pramudita, G.N. Precise Topographic Mapping Using Direct Georeferencing in UAV. *IOP Conf. Ser. Earth Environ. Sci.* **2020**, *500*, 12029. [CrossRef]
56. De Jesús, A.; Breña-Naranjo, J.A.; Pedrozo-Acuña, A.; Alcocer Yamanaka, V.H. The Use of TRMM 3B42 Product for Drought Monitoring in Mexico. *Water* **2016**, *8*, 325. [CrossRef]
57. DJI Ground Station Pro. Available online: <https://www.dji.com/mx/ground-station-pro> (accessed on 3 April 2023).
58. OpenDroneMap Awesome. Drone. Software. Available online: www.opendronemap.org (accessed on 2 April 2023).
59. Groos, A.R.; Bertschinger, T.J.; Kummer, C.M.; Erlwein, S.; Munz, L.; Philipp, A. The Potential of Low-Cost UAVs and Open-Source Photogrammetry Software for High-Resolution Monitoring of Alpine Glaciers: A Case Study from the Kanderfirn (Swiss Alps). *Geosciences* **2019**, *9*, 356. [CrossRef]
60. Deliry, S.I.; Avdan, U. Accuracy of Unmanned Aerial Systems Photogrammetry and Structure from Motion in Surveying and Mapping: A Review. *J. Indian Soc. Remote Sens.* **2021**, *49*, 1997–2017. [CrossRef]
61. Iglhaut, J.; Cabo, C.; Puliti, S.; Piermattei, L.; O'Connor, J.; Rosette, J. Structure from Motion Photogrammetry in Forestry: A Review. *Curr. For. Rep.* **2019**, *5*, 155–168. [CrossRef]
62. Zhang, W.; Qi, J.; Wan, P.; Wang, H.; Xie, D.; Wang, X.; Yan, G. An Easy-to-Use Airborne LiDAR Data Filtering Method Based on Cloth Simulation. *Remote Sens.* **2016**, *8*, 501. [CrossRef]
63. Lee, S.; Yu, B.-H. Automatic Detection of Dead Tree from UAV Imagery. In Proceedings of the 39th Asian Conference on Remote Sensing, Kuala Lumpur, Malaysia, 15–19 October 2018.
64. Rosas-Chavoya, M.; Gallardo-Salazar, J.L.; López-Serrano, P.M.; Alcántara-Concepción, P.C.; León-Miranda, A.K. QGIS a Constantly Growing Free and Open-Source Geospatial Software Contributing to Scientific Development. *Cuad. Investig. Geográfica* **2022**, *48*, 197–213. [CrossRef]
65. Minařík, R.; Langhammer, J.; Lendzioch, T. Automatic Tree Crown Extraction from UAS Multispectral Imagery for the Detection of Bark Beetle Disturbance in Mixed Forests. *Remote Sens.* **2020**, *12*, 4081. [CrossRef]
66. Jones, H.G.; Vaughan, R.A. *Remote Sensing of Vegetation: Principles, Techniques, and Applications*; Oxford University Press: Oxford, UK, 2010; ISBN 0199207798.
67. Liu, S.; Zeng, W.; Wu, L.; Lei, G.; Chen, H.; Gaiser, T.; Srivastava, A.K. Simulating the Leaf Area Index of Rice from Multispectral Images. *Remote Sens.* **2021**, *13*, 3663. [CrossRef]
68. Narmilan, A.; Gonzalez, F.; Salgadoe, A.S.A.; Kumarasiri, U.W.L.M.; Weerasinghe, H.A.S.; Kulasekara, B.R. Predicting Canopy Chlorophyll Content in Sugarcane Crops Using Machine Learning Algorithms and Spectral Vegetation Indices Derived from UAV Multispectral Imagery. *Remote Sens.* **2022**, *14*, 1140. [CrossRef]
69. Nevalainen, O.; Honkavaara, E.; Tuominen, S.; Viljanen, N.; Hakala, T.; Yu, X.; Hyypä, J.; Saari, H.; Pölönen, I.; Imai, N.N.; et al. Individual Tree Detection and Classification with UAV-Based Photogrammetric Point Clouds and Hyperspectral Imaging. *Remote Sens.* **2017**, *9*, 185. [CrossRef]
70. Mohan, M.; Leite, R.V.; Broadbent, E.N.; Wan Mohd Jaafar, W.S.; Srinivasan, S.; Bajaj, S.; Dalla Corte, A.P.; do Amaral, C.H.; Gopan, G.; Saad, S.N.M.; et al. Individual Tree Detection Using UAV-Lidar and UAV-SfM Data: A Tutorial for Beginners. *Open Geosci.* **2021**, *13*, 1028–1039. [CrossRef]
71. Gallardo-Salazar, J.L.; Pompa-García, M. Detecting Individual Tree Attributes and Multispectral Indices Using Unmanned Aerial Vehicles: Applications in a Pine Clonal Orchard. *Remote Sens.* **2020**, *12*, 4144. [CrossRef]
72. Picos, J.; Bastos, G.; Míguez, D.; Alonso, L.; Armesto, J. Individual Tree Detection in a Eucalyptus Plantation Using Unmanned Aerial Vehicle (UAV)-LiDAR. *Remote Sens.* **2020**, *12*, 885. [CrossRef]
73. Crabbé, A.; Cahy, T.; Somers, B.; Verbeke, L.P.; Van Coillie, F. Tree Density Calculator Software. Available online: <https://bitbucket.org/kul-reseco/localmaxfilter> (accessed on 2 April 2023).
74. Ke, Y.; Quackenbush, L.J. A Review of Methods for Automatic Individual Tree-Crown Detection and Delineation from Passive Remote Sensing. *Int. J. Remote Sens.* **2011**, *32*, 4725–4747. [CrossRef]
75. Li, W.; Fu, H.; Yu, L.; Cracknell, A. Deep Learning Based Oil Palm Tree Detection and Counting for High-Resolution Remote Sensing Images. *Remote Sens.* **2017**, *9*, 22. [CrossRef]
76. Jiménez, J.; Aguirre, O.; Kramer, H. Tree Crown Structure Indicators in a Natural Uneven-Aged Mixed Coniferous Forest in Northeastern Mexico. In Proceedings of the Monitoring Science and Technology Symposium: Unifying Knowledge for Sustainability in the Western Hemisphere Proceedings RMRS-P-42CD; Department of Agriculture, Forest Service, Rocky Mountain Research Station: Fort Collins, CO, USA, 2006; pp. 649–654.

77. Zhang, J.; You, S.; Gruenwald, L. Efficient Parallel Zonal Statistics on Large-Scale Global Biodiversity Data on GPUs. In Proceedings of the 4th International ACM SIGSPATIAL Workshop on Analytics for Big Geospatial Data, Bellevue, WA, USA, 3–6 November 2015; Association for Computing Machinery: New York, NY, USA, 2015; pp. 35–44.
78. Buras, A.; Schunk, C.; Zeitrag, C.; Herrmann, C.; Kaiser, L.; Lemme, H.; Straub, C.; Taeger, S.; Gößwein, S.; Klemmt, H.-J.; et al. Are Scots Pine Forest Edges Particularly Prone to Drought-Induced Mortality? *Environ. Res. Lett.* **2018**, *13*, 025001. [CrossRef]
79. Ye, H.; Huang, W.; Huang, S.; Cui, B.; Dong, Y.; Guo, A.; Ren, Y.; Jin, Y. Recognition of Banana Fusarium Wilt Based on UAV Remote Sensing. *Remote Sens.* **2020**, *12*, 938. [CrossRef]
80. Alley, W.M. The Palmer Drought Severity Index: Limitations and Assumptions. *J. Clim. Appl. Meteorol.* **1984**, *23*, 1100–1109. [CrossRef]
81. Gómez-Pineda, E.; Hammond, W.M.; Trejo-Ramirez, O.; Gil-Fernández, M.; Allen, C.D.; Blanco-García, A.; Sáenz-Romero, C. Drought Years Promote Bark Beetle Outbreaks in Mexican Forests of *Abies religiosa* and *Pinus pseudostrobus*. *For. Ecol. Manag.* **2022**, *505*, 119944. [CrossRef]
82. Abatzoglou, J.T.; Dobrowski, S.Z.; Parks, S.A.; Hegewisch, K.C. TerraClimate, a High-Resolution Global Dataset of Monthly Climate and Climatic Water Balance from 1958–2015. *Sci. Data* **2018**, *5*, 170191. [CrossRef]
83. R Core Team. *R: A Language and Environment for Statistical Computing*; R Foundation for Statistical Computing: Vienna, Austria, 2023.
84. He, J.; Li, Y.; Zhang, K. Research of UAV Flight Planning Parameters. *Positioning* **2012**, *3*, 43–45. [CrossRef]
85. Carrillo-Arizmendi, L.; Pérez-Suárez, M.; Vargas-Hernández, J.J.; Rozenberg, P.; Martínez-Campos, A.R. Warming Effects on Tree-Ring Variables in *P. hartwegii* Lindl. at the Extremes of Its Natural Elevational Distribution in Central Mexico. *Agric. For. Meteorol.* **2022**, *324*, 109109. [CrossRef]
86. Sexton, J.P.; McIntyre, P.J.; Angert, A.L.; Rice, K.J. Evolution and Ecology of Species Range Limits. *Annu. Rev. Ecol. Evol. Syst.* **2009**, *40*, 415–436. [CrossRef]
87. Mátyás, C.; Berki, I.; Bidló, A.; Csóka, G.; Czimber, K.; Führer, E.; Gálos, B.; Gribovszki, Z.; Illés, G.; Hirka, A.; et al. Sustainability of Forest Cover under Climate Change on the Temperate-Continental Xeric Limits. *Forests* **2018**, *9*, 489. [CrossRef]
88. Mátyás, C.; BERKI, I.; Czúcz, B.; Gálos, B.; Móricz, N.; Rasztovits, E. Future of Beech in Southeast Europe from the Perspective of Evolutionary Ecology. *Acta Silv. Lignaria Hung.* **2010**, *6*, 91–110.
89. Ricker, M.; Gutiérrez-García, G.; Daly, D.C. Modeling Long-Term Tree Growth Curves in Response to Warming Climate: Test Cases from a Subtropical Mountain Forest and a Tropical Rainforest in Mexico. *Can. J. For. Res.* **2007**, *37*, 977–989. [CrossRef]
90. Choat, B.; Brodribb, T.J.; Brodersen, C.R.; Duursma, R.A.; López, R.; Medlyn, B.E. Triggers of Tree Mortality under Drought. *Nature* **2018**, *558*, 531–539. [CrossRef]
91. Cambrón-Sandoval, V.H.; Méndez-González, J.; Ledesma-Colunga, M.C.; Luna-Soria, H.; García-Aranda, M.A.; Cerano-Paredes, J.; Obregón-Zúñiga, J.A.; Vergara-Pineda, S. *Variabilidad Climática e Interacción con Otros Factores que Afectan la Dinámica Poblacional de Descortezadores en Bosques Amenazados de México*; CONAFOR-CONACYT: Querétaro, Mexico, 2018; ISBN 978-607-513-336-2.
92. Tejeda-Landero, V.M.; Sánchez-Velásquez, L.R.; Viveros-Viveros, H.; Aparicio-Rentería, A.; Flores-Pereido, R. Seed Bank Formation and Removal of *Pinus hartwegii* (Pinaceae) Seeds along an Altitudinal Gradient in the Cofre de Perote National Park, Veracruz, Mexico. *Bot. Sci.* **2019**, *97*, 623–629. [CrossRef]
93. Alba-Landa, J.; Aparicio-Rentería, A.; Márquez-Ramírez, J. Potencial y eficiencia de producción de semillas de *Pinus hartwegii* lindl. de dos poblaciones de México. *For. Veracruzana* **2003**, *5*, 25–28.
94. Astudillo-Sánchez, C.C.; Fowler, M.S.; Villanueva-Díaz, J.; Endara-Agramont, A.R.; Soria-Díaz, L. Recruitment and Facilitation in *Pinus hartwegii*, a Mexican Alpine Treeline Ecotone, with Potential Responses to Climate Warming. *Trees* **2019**, *33*, 1087–1100. [CrossRef]
95. Castellanos-Acuña, D.; Vance-Borland, K.W.; St. Clair, J.B.; Hamann, A.; López-Upton, J.; Gómez-Pineda, E.; Ortega-Rodríguez, J.M.; Sáenz-Romero, C. Climate-Based Seed Zones for Mexico: Guiding Reforestation under Observed and Projected Climate Change. *New For.* **2018**, *49*, 297–309. [CrossRef]
96. Manzanilla-Quiñones, U.; Aguirre-Calderón, Ó.A.; Jiménez-Pérez, J.; Treviño-Garza, E.J.; Yerena-Yamallel, J.I. Distribución Actual y Futura Del Bosque Subalpino de *Pinus hartwegii* Lindl En El Eje Neovolcánico Transversal. *Madera Bosques* **2019**, *25*. [CrossRef]
97. Millar, C.I.; Stephenson, N.L. Temperate Forest Health in an Era of Emerging Megadisturbance. *Science* **2015**, *349*, 823–826. [CrossRef]
98. Hill, A.P.; Nolan, C.J.; Hemes, K.S.; Cambron, T.W.; Field, C.B. Low-Elevation Conifers in California’s Sierra Nevada Are out of Equilibrium with Climate. *PNAS Nexus* **2023**, *2*, pgad004. [CrossRef]
99. Minařík, R.; Langhammer, J. Use of a Multispectral UAV Photogrammetry for Detection and Tracking of Forest Disturbance Dynamics. *Int. Arch. Photogramm. Remote Sens. Spat. Inf. Sci.* **2016**, *XLI-B8*, 711–718. [CrossRef]
100. Cristiano, P.; Madanes, N.; Campanello, P.; di Francescantonio, D.; Rodriguez, S.; Zhang, Y.-J.; Carrasco, L.; Goldstein, G. High NDVI and Potential Canopy Photosynthesis of South American Subtropical Forests despite Seasonal Changes in Leaf Area Index and Air Temperature. *Forests* **2014**, *5*, 287–308. [CrossRef]
101. Gamon, J.A.; Kovalchuck, O.; Wong, C.Y.S.; Harris, A.; Garrity, S.R. Monitoring Seasonal and Diurnal Changes in Photosynthetic Pigments with Automated PRI and NDVI Sensors. *Biogeosciences* **2015**, *12*, 4149–4159. [CrossRef]
102. Rullan-Silva, C.D.; Olthoff, A.E.; Delgado de la Mata, J.A.; Pajares-Alonso, J.A. Remote Monitoring of Forest Insect Defoliation—A Review. *For. Syst.* **2013**, *22*, 377. [CrossRef]

103. Di Bella, C.M.; Paruelo, J.M.; Becerra, J.E.; Bacour, C.; Baret, F. Effect of Senescent Leaves on NDVI-Based Estimates of FAPAR: Experimental and Modelling Evidences. *Int. J. Remote Sens.* **2004**, *25*, 5415–5427. [[CrossRef](#)]
104. Chavana-Bryant, C.; Malhi, Y.; Wu, J.; Asner, G.P.; Anastasiou, A.; Enquist, B.J.; Cosio Caravasi, E.G.; Doughty, C.E.; Saleska, S.R.; Martin, R.E.; et al. Leaf Aging of Amazonian Canopy Trees as Revealed by Spectral and Physiochemical Measurements. *New Phytol.* **2017**, *214*, 1049–1063. [[CrossRef](#)]
105. Yao, H.; Qin, R.; Chen, X. Unmanned Aerial Vehicle for Remote Sensing Applications—A Review. *Remote Sens.* **2019**, *11*, 1443. [[CrossRef](#)]
106. Puliti, S.; Breidenbach, J.; Astrup, R. Estimation of Forest Growing Stock Volume with UAV Laser Scanning Data: Can It Be Done without Field Data? *Remote Sens.* **2020**, *12*, 1245. [[CrossRef](#)]
107. Gonroudobou, O.B.H.; Silvestre, L.H.; Diez, Y.; Nguyen, H.T.; Caceres, M.L.L. Treetop Detection in Mountainous Forests Using UAV Terrain Awareness Function. *Computation* **2022**, *10*, 90. [[CrossRef](#)]
108. LaRue, E.A.; Fahey, R.T.; Alveshere, B.C.; Atkins, J.W.; Bhatt, P.; Buma, B.; Chen, A.; Cousins, S.; Elliott, J.M.; Elmore, A.J.; et al. A Theoretical Framework for the Ecological Role of Three-dimensional Structural Diversity. *Front. Ecol. Environ.* **2023**, *21*, 4–13. [[CrossRef](#)]

Disclaimer/Publisher’s Note: The statements, opinions and data contained in all publications are solely those of the individual author(s) and contributor(s) and not of MDPI and/or the editor(s). MDPI and/or the editor(s) disclaim responsibility for any injury to people or property resulting from any ideas, methods, instructions or products referred to in the content.